Quaternary International 479 (2018) 106–116

Contents lists available at ScienceDirect

Quaternary International

journal homepage: www.elsevier.com/locate/quaint

# Geochemical characteristics of surface dune sand in the Mu Us Desert, Inner Mongolia, and implications for reconstructing the paleoenvironment

Peixian Shu [a, b, d], Baosheng Li [a, c, *], Hong Wang [d], Yahui Qiu [e], Dongfeng Niu [c], David Dianzhang [f], Zhisheng An [a]

[a] State Key Laboratory of Loess and Quaternary Geology, Institute of Earth Environment, Chinese Academy of Sciences, Xi'an 710061, China
[b] University of Chinese Academy of Sciences, Beijing 100049, China
[c] School of Geography, South China Normal University, Guangzhou 510631, China
[d] Illinois State Geological Survey, Prairie Research Institute, University of Illinois at Urbana-Champaign, 615 E. Peabody Drive, Champaign 61820, USA
[e] Institute of Cenozoic Geology and Environment, State Key Laboratory of Continental Dynamics, Department of Geology, Northwest University, Xi'an 710069, China
[f] Department of Geography, University of Hong Kong, Hong Kong, China

ARTICLE INFO

*Article history:*
Received 31 October 2016
Accepted 2 May 2017
Available online 16 June 2017

*Keywords:*
Mu Us Desert
Dune sands
Geochemistry
Paleoenvironment

ABSTRACT

We present a new dataset from 28 active and 13 stabilized–semi stabilized dunefields in the Mu Us Desert to report the geochemical macroscale properties as well as reveal the relationship between various chemical ratios and modern climate conditions among different types of Mu Us sandy landscapes. We find that several chemical-weathering indexes, such as CIA, CIW, CPA, and WIP, can be used for the reconstruction of the paleoclimate and servel conditions. One should be cautious in interpreting the weathering intensity using these chemical ratios at a given deposition site when the geochemical background is unknown. This preliminary geochemistry study shows that stabilized–semi stabilized dunefields, which are influenced by Asian summer monsoon (ASM) precipitation, are analogous to buried paleosols, whereas active dunefields, which are controlled by Asian winter monsoon (AWM) wind, resemble paleo-dune sand. The comparison with the geochemical results from an excellent dune–paleosol succession implies that stronger ASM and AWM periods could have recurred 8–9 times in the Mu Us Desert during the early Holocene.



## 1. Introduction

Massive dunefields cover up to 810,000 km$^2$ of northern China (Wu, 2009; Zhu et al., 1980). The Mu Us desert (also be called Mu us sandy land) is one of the key regions for studying the history of eolian sand activity and the evolution of the desert in northern China (Dong et al., 2002). Dong et al. (1983) identified ancient eolian sands for the first time in the Mu Us region. And then they attributed the multiple alternations of the eolian dune sand and lacustrine deposits observed in the Salawusu Basin of the Mu Us Desert to the orbital-scale paleomonsoon strength (Dong et al., 1998; Li et al., 2000). The loess–eolian sand sequence at the southern margin of the Mu Us Desert confirmed the link between the enlargement and reduction of the dunefield and the paleomonsoon strength further (Ding et al., 1999; Li et al., 2005; Liu and Sun, 2002; Sun et al., 1999). In the past few decades, a growing number of optically stimulated luminescence data derived from dune sand–paleosol records have provided good chronological knowledge of the servelal changes in the Mu Us region (He et al., 2010; Jia et al., 2015; Li et al., 2012; Liu et al., 2014; Liu and Lai, 2012; Lu et al., 2005; Wen et al., 2016; Xu et al., 2015a). However, the link between dunefield formation and insolation forcing is not always straightforward (Lu et al., 2005) and is inconsistent with other dune records form other locations (Thomas and Burrough, 2013), which may demonstrate a nonlinear relationship between climate change and dune system response (Duller, 2016; Halfen et al., 2016; Lancaster et al., 2013; Li and Yang, 2016). While the lack of an independent climate proxy in coarse-grained dune sand

* Corresponding author. School of Geography, South China Normal University, Guangzhou 510631, China.
*E-mail address:* libsh2013@163.com (B. Li).

http://dx.doi.org/10.1016/j.quaint.2017.05.053
1040-6182/

(Fitzsimmons et al., 2013), such as the pollen spectrum (Lu et al., 2012), hinders the quantification/semi-quantification of specific paleoenvironment changes in sand region (Lancaster, 2008; Telfer and Hesse, 2013; Thomas and Burrough, 2012). Some geochemical proxies obtained from eolian loess–paleosol deposits provide useful information regarding the reconstruction of the paleoenvironment (Li et al., 2008; Wang et al., 2008; Yang et al., 2006), however, because source detritus, grain size variation and sediment transport process could alter the geochemical composition, especially in the desert, the uncertainty of the reconstruction of the paleoenvironment and climate sometimes increase to a level at which the interpretation is no longer valid.

The goal of this study is to characterize the chemical properties of active and stabilized dunefields of the Mu Us Desert to develop a modern analog for reconstructing servel and paleoclimate. We investigated chemical properties of active and stabilized dunefields of the Mu Us Desert as well as the regional variation at the macroscopic scale by presenting a new dataset from 28 active (MMD) and 13 stabilized–semi stabilized (MFD) dunefields in the Mu Us Desert. And revealing the relationship between various chemical weathering indexes and modern climate conditions among different types of Mu Us sandy landscape. We find several potential parameters for using in the reconstruction of the paleoclimate and servel conditions.

## 2. Area description

The Mu Us sandy region is located between the Ordos Plateau and Loess Plateau and mainly lies in the southeastern depression. Some dunefields cover the Ordos Plateau and partly expand into the northwestern margin of the Loess Plateau. This desert, covering more than 40,000 km$^2$, is one of the four largest sandy regions in eastern China (Wu, 2009). Fully active and vegetation-stabilized dunes coexist, as indicated by a remote sensing image (Fig. 1). It shows active dunefields occupying the uplands and stabilized dunefields predominating low-lying depressions, valleys, and lake margins. The active dunes are composed of crescent barchanoid ridges and parabolic, honeycomb, and nabkha dunes.

The current weather in the Mu Us Desert is strongly influenced by the Asian summer monsoon (ASM) and Mongolia–Siberia high-pressure cell systems. The mean annual precipitation of the southeastern sector is 400–450 mm and declines to 250 mm toward the northwestern sector, while the mean annual temperature of the region ranges between 6 °C and 9 °C (Xu et al., 2015b). It is warm and semi-humid in summer and cold and dry in winter. During summer and fall, the southeasterly winds of the ASM prevail and semi-humid conditions support a healthy ecosystem. During winter and spring, northerly and northwesterly winds of the Asian winter monsoon prevail and drier, colder, windier, and dustier conditions inhibit plant growth. Wind erosion and eolian transportation mainly occur during winter and spring.

## 3. Methods and material studied

We collected 28 surface sand samples from active dunefields and 13 samples from stabilized and semi-stabilized dunefields. Active dunefield samples were recovered from barchan sand dunes at the upper apex of the upland, and stabilized and semi-stabilized samples were recovered from the top of nabkha sand dunes in low-lying depressions and basins. All samples were collected at a depth of 1–5 cm below the land surface. We used differential GPS (mode: S750-G2) to record the geographic coordinates and elevation and employed an ArcGIS10 projection of the location (Fig. 1).

The elemental concentrations of 41 samples were measured using a polarized energy-dispersive X-ray fluorescence spectrometer (mode: Epsilon 5). All samples were dried in a low-temperature (38 °C) oven for 72 h, passed through a 2-mm sieve, and ground to < 75 μm (200-mesh) using a ZHM-1A shatter box for 90 s. Six grams of each pulverized sample was compacted into a disc with a diameter of 3.2 cm using 30-ton pressure for 30 s. A calibration curve was developed using 27 Chinese national soil reference materials (GSS2 to GSS28), 6 fluvial sediment reference materials (GSD2a, GSD7a, and GSD9 to GSD12), and 6 rock reference materials (GSR1 to GSR6). The repeatability of the elemental measurements was evaluated through duplicate analyses of the National Standard soil reference GSS17. The experimental analytical uncertainty of the major elements was ±5% and that of the trace elements was less than 10%. The major elements are given in the form of oxides in wt%. The analytical results are shown in Table 1.

Particle size analysis was performed using a Mastersizer 2000 M

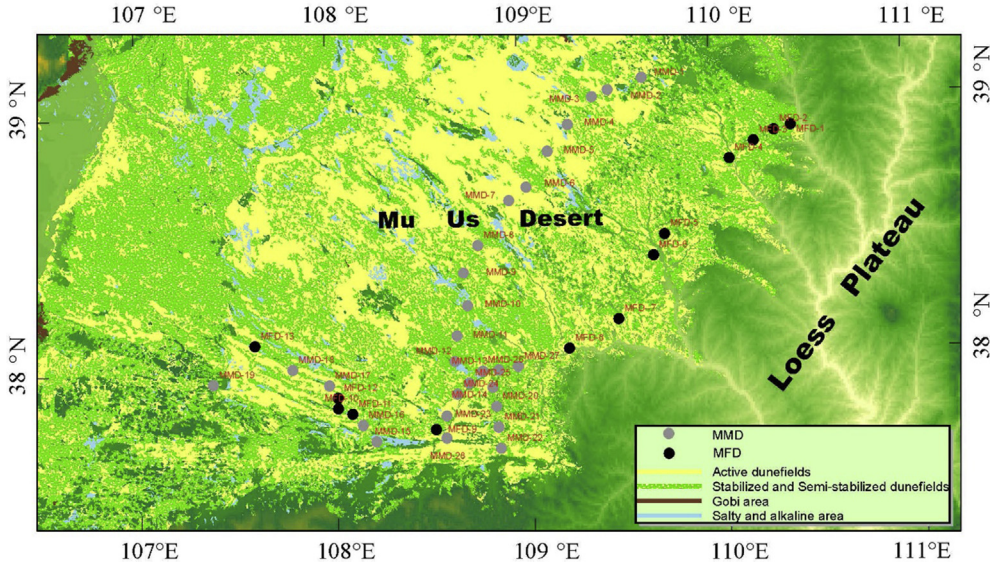


**Fig. 1.** Locations of dune sand samples in the Mu Us Desert. The satellite image data are provided by the International Scientific & Technical Data Mirror Site, Computer Network Information Center and the Chinese Academy of Sciences.

**Table 1**
Dating results of accelerator mass spectrometry (AMS) $^{14}C$ from bulk samples of the shenmu section.

| Horizon | Depth(cm) | Lab. no. | Dated materials | $\delta^{13}C$ (‰) | $^{14}C$ age (yr BP) | Calibrated age (yr BP, ±2σ error) |
|---|---|---|---|---|---|---|
| 1BS | 14 | Beta 429449 | Organic matter | −22.50 | 5540 ± 30 | 6350 ± 50 |
| 3BS | 96 | XA961 | Organic matter | −23.47 | 6846 ± 36 | 7684 ± 76 |
| 5BS | 150 | Beta 429450 | Organic matter | −22.90 | 7860 ± 30 | 8670 ± 90 |
| (Parker, 1970) | 197 | XA958 | Organic matter | −20.23 | 7472 ± 33 | 8324 ± 49 |
| 11BS | 258 | Beta 429451 | Organic matter | −22.70 | 7730 ± 30 | 8500 ± 70 |
| 13BS | 290 | XA953 | Organic matter | −19.78 | 8533 ± 37 | 9513 ± 32 |
| 15BS | 314 | XA955 | Organic matter | −24.14 | 8724 ± 35 | 9675 ± 122 |
| 19BS | 398 | XA956 | Organic matter | −22.59 | 9237 ± 35 | 10,391 ± 120 |
| 20PD | 437 | XA952 | Organic matter | −22.64 | 9532 ± 48 | 10,800 ± 110 |

laser particle analyzer, which has a measuring range of 0.02 μm–2000 μm. We calculated the Mz (mean particle diameter) and σ (standard deviation) in $Mz = (\Phi16 + \Phi50 + \Phi84)/3$; $\sigma = (\Phi84 - \Phi16)/4 + (\Phi95 - \Phi5)/6.6$ and $\Phi = -\log_2 d$ (Folk and Ward, 1957).

We also collected 243 sequential samples from an excellent dune–paleosol succession in the Shenmu City area. This 4.5 m long succession contains 20 sedimentary units, including 10 layers of paleo-eolian sands alternating with 10 layers of sandy paleosols (better known to the natives as sandy black loams). The dune sand units are composed of brownish (Munsell 10 YR 5/8) uniform fine–medium sand. The paleosol horizons consist of black-brown silty loam (Munsell 7.5 YR 4/4) with fine sand. Nine $^{14}C$ samples from the Shenmu section was used to date at the Xi'an AMS laboratory, China, and at Beta Analytic Inc., Florida, USA, using standard Accelerator Mass Spectrometry delivery analysis, which results have been reported recently and shown in Table 1 (Wen et al., 2016).

## 4. Results and analyses

### 4.1. Geochemical composition

Silicon and aluminum dominate the geochemical composition of the surface sand samples from the Mu Us Desert. The Si contents range from 67% to 90%, with an average value of 80%, and the Al concentrations vary between 6.7% and 12.0%, with an average value of 9.5% (Table 2). The average contents of Na, K, Fe, and Ca range between 1% and 2.5%, while the Mg and Ti contents are below 1% (Table 2).

We selected a total of 12 trace elements, including Ba, Sr, Zr, Rb, Co, Ni, Cr, Cu, V, Ga, Nb, and Ge, to characterize the different types of dunefields in the Mu Us Desert (Table 2). The Zr, Ba, and Sr contents are higher than those of other trace elements (Table 2). Barium shows the highest content, with an average of 645.9 ppm, ranging from 379 to 948 ppm. The average content of Sr is 228.4 ppm, ranging from 100 to 391 ppm, while the Zr content has an average of 145.6 ppm, ranging from 63 to 298 ppm. Other trace elements show average contents below 100 ppm (Table 2).

The major elements contents of active and stabilized and semi-stabilized dunefields differ in certain ways. The Si content of active dunefields is 7.5% higher than that of stabilized and semi-stabilized dunefields. By contrast, the average, maximum, and minimum Al, Fe, Ca, Mg, and Ti contents are lower in active dunefields than in stabilized and semi-stabilized dunefields. However, the average and minimum contents of K and Na are higher in active dunefields. All of the elements coefficients of variation are greater in active dunefields than in stabilized and semi-stabilized dunefields, except for Si and Ca (Table 2).

The Ba and Sr abundance is 40 ppm and 10 ppm in active dunefields higher than in the stabilized and semi-stabilized dunefields, respectively, and the Ge and Ni element contents are very similar. The rest of the elements show higher contents in stabilized and semi-stabilized dunefields. The coefficient of variation (CV) values of Ba, Sr, Ni, Cu, and Ga of active dunefields are lower than those of stabilized and semi-stabilized dunefields.

### 4.2. Geochemical characteristics

Comparison of the average chemical composition of the major elements shows that Si is enriched and other elements are depleted in the upper continental crust (UCC, Taylor and McLennan, 1985). Comparison of the average chemical composition of the trace elements indicates that Ba, Co, and Ge are relatively enriched and other trace elements are relatively depleted. When comparing the trace element contents of active dune sands and stabilized and semi-stabilized dune sands, elements are depleted, except for Ba and Sr (Fig. 2).

In geochemistry, A–CN–K ternary diagrams are widely accepted

**Table 2**
Major elements in Mu Us Desert samples (%).

| Samples | Parameter | $SiO_2$ | $Al_2O_3$ | $Fe_2O_3$ | CaO | $Na_2O$ | MgO | $K_2O$ | $TiO_2$ | Ba | Sr | Zr | Rb | Co | V | Ni | Cr | Cu | Ga | Nb | Ge |
|---|---|---|---|---|---|---|---|---|---|---|---|---|---|---|---|---|---|---|---|---|---|
| | unit | % | % | % | % | % | % | % | % | ppm | ppm | ppm | ppm | ppm | ppm | ppm | ppm | ppm | ppm | ppm | ppm |
| All (n = 41) | average | 80.35 | 9.47 | 1.70 | 1.32 | 2.33 | 0.49 | 2.31 | 0.16 | 645 | 228 | 145 | 65.6 | 26.9 | 31.2 | 18.7 | 22.5 | 7.48 | 7.74 | 7.95 | 5.69 |
| | minimum | 67.51 | 6.69 | 0.70 | 0.56 | 1.35 | 0.01 | 1.72 | 0.06 | 379 | 100 | 63.0 | 53.0 | 12.6 | 10.0 | 7.60 | 3.00 | 3.50 | 2.60 | 6 | 0.61 |
| | maximum | 90.47 | 11.99 | 2.60 | 2.85 | 3.31 | 1.13 | 2.93 | 0.26 | 948 | 391 | 298 | 80.0 | 39.3 | 63.0 | 32.6 | 48.0 | 13.1 | 12.2 | 10.9 | 8.47 |
| | CV | 0.08 | 0.16 | 0.27 | 0.38 | 0.24 | 0.46 | 0.17 | 0.27 | 0.30 | 0.40 | 0.42 | 0.11 | 0.23 | 0.30 | 0.43 | 0.45 | 0.31 | 0.39 | 0.13 | 0.26 |
| MMD (n = 28) | average | 82.54 | 9.25 | 1.49 | 1.11 | 2.39 | 0.4 | 2.33 | 0.15 | 657 | 231 | 121 | 64.2 | 27.1 | 27.0 | 18.8 | 17.7 | 6.85 | 7.49 | 7.46 | 5.79 |
| | minimum | 74.99 | 6.69 | 0.70 | 0.56 | 1.35 | 0.01 | 1.72 | 0.06 | 379 | 100 | 63.0 | 53.0 | 12.6 | 10.0 | 7.60 | 3.00 | 3.5 | 2.6 | 6 | 2.43 |
| | maximum | 90.47 | 11.99 | 2.10 | 1.76 | 3.31 | 0.85 | 2.93 | 0.21 | 948 | 391 | 210 | 73.0 | 39.3 | 36.0 | 32.6 | 34.0 | 10.3 | 12.2 | 8.7 | 8.47 |
| | CV | 0.05 | 0.16 | 0.21 | 0.30 | 0.26 | 0.40 | 0.19 | 0.21 | 0.31 | 0.42 | 0.31 | 0.11 | 0.25 | 0.21 | 0.44 | 0.41 | 0.32 | 0.42 | 0.09 | 0.24 |
| MFD (n = 13) | average | 75.06 | 10.02 | 2.23 | 1.82 | 2.19 | 0.72 | 2.29 | 0.21 | 618 | 221 | 204 | 68.8 | 26.4 | 41.4 | 18.4 | 33.9 | 9.01 | 8.34 | 9.14 | 5.44 |
| | minimum | 67.51 | 6.92 | 1.70 | 0.83 | 1.59 | 0.48 | 1.73 | 0.15 | 405 | 125 | 112 | 54.0 | 18.0 | 29.0 | 10.5 | 27.0 | 5.4 | 3.6 | 7.6 | 0.61 |
| | maximum | 88.81 | 11.87 | 2.60 | 2.85 | 2.59 | 1.13 | 2.66 | 0.26 | 813 | 311 | 298 | 80.0 | 37.3 | 63.0 | 30.8 | 48.0 | 13.1 | 11.9 | 10.9 | 7.68 |
| | CV | 0.09 | 0.15 | 0.12 | 0.27 | 0.15 | 0.26 | 0.13 | 0.17 | 0.26 | 0.31 | 0.33 | 0.10 | 0.20 | 0.22 | 0.40 | 0.18 | 0.21 | 0.3 | 0.1 | 0.32 |

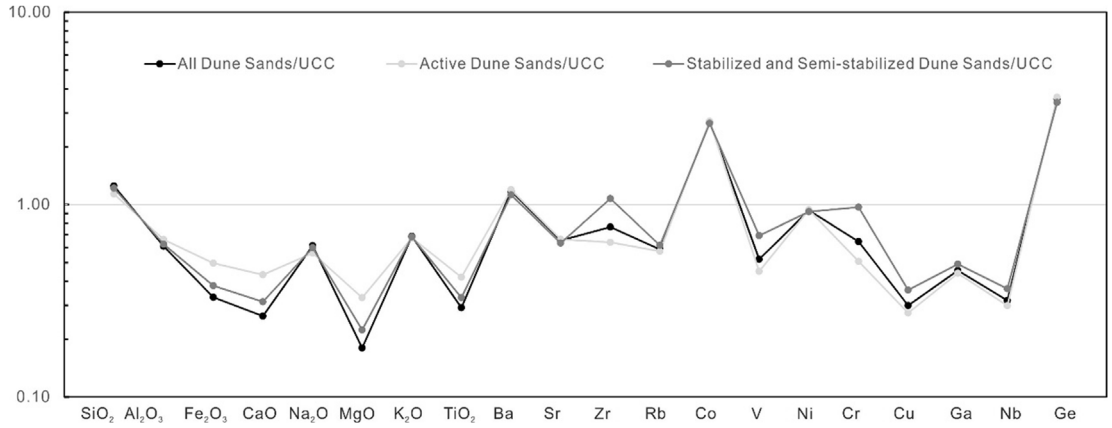


**Fig. 2.** UCC-normalized curves of the average contents of the Mu Us Desert dune sand elements.

as indicators of continental chemical weathering trends (Chen et al., 2001; Nesbitt and Young, 1982). Here, A is the $Al_2O_3$ content, C is the CaO content, N is the $Na_2O$ content, and K is the $K_2O$ content. The trendline from UCC to post-Archean Australian shale (PAAS) indicates an early stage of weathering. The active dunefield samples of the Mu Us Desert show elemental concentrations around or below the UCC values (Fig. 2) with slightly leached Na and Ca contents, implying that the samples did not experience significant chemical weathering. The stabilized and semi-stabilized dunefield samples show somewhat higher elemental concentrations than those of the UCC, which indicates stronger weathering. In general, the surface dune sands of this desert lack in effective chemical weathering, as shown by the A–CN–K ternary diagram (Fig. 3).

## 5. Discussion

### 5.1. Provenance and deposition sorting effect on the geochemical composition

General speaking, weathering, provenance and deposition sorting are important factors affecting the chemical composition of eoiian sediments (Yang et al., 2006). We start with considering that the provenance factor, aiming at to identify the dune sand source. Due to stabilized dune are fixed by the plant from active dune in this region (Xu et al., 2015b), and we supposed both stabilized and active dunefields share the same provenance. While stabilized dune experienced weathering by biochemical more or less. Thus, we chose the trace elements in active dunefields that reflect the geochemical fingerprint of the source areas, and their contents are

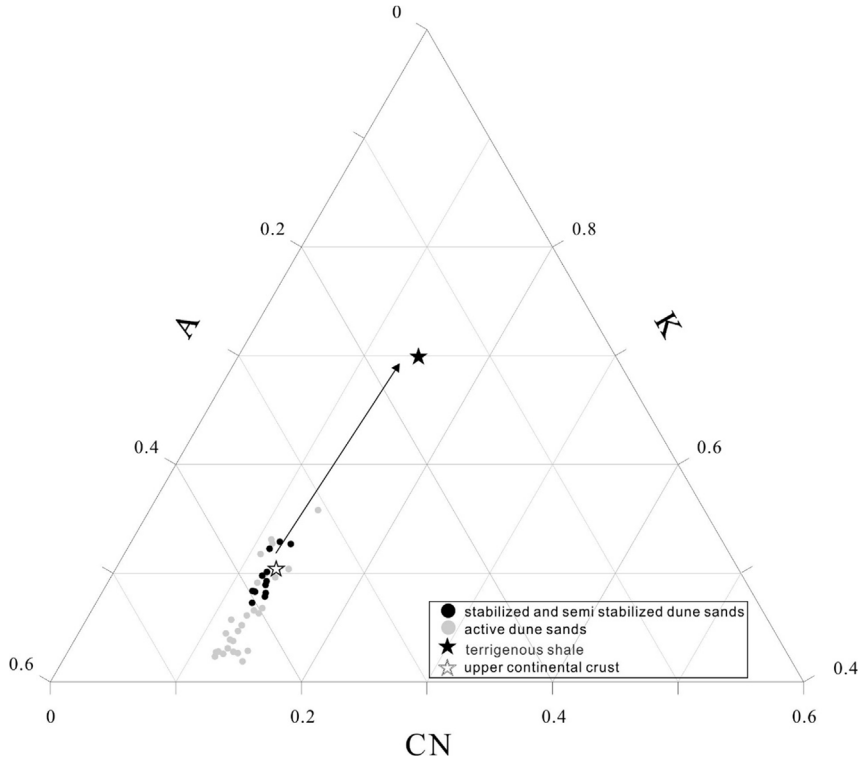


**Fig. 3.** A–CN–K ternary diagram of Mu Us Desert dune sands. A is $Al_2O_3$, C is CaO*, N is $Na_2O$, K is $K_2O$. CaO *: molar content of carbonate in silicate minerals. The calculation process follows the method of Honda and Shimizu (1998). UCC and PAAS data are from Taylor and McLennan (1985).

consistent with the UCC value (Fig. 4). It can been seen that the HMD1–HMD10 sites show a relatively consistent variation, as characterized by higher Ba, Go, and Ge concentrations, which are defined here as group one (Fig. 4a). The MMD16–MMD19, MMD21, MMD23, MMD24, and MMD26–MMD28 sites show similar patterns, with higher Ni, Go, and Ge concentrations (Fig. 4b and c), and are defined as group two. The MMD12–MMD15, MMD20, MMD22, and MMD25 sites, called group three, show different trends of element changes (Fig. 4d) and their mixed chemical characteristics suggest multiple sources. Thus, at least two endmembers are identified from different provenances in the study area.

Active dunefields in the northeastern Mu Us Desert have a similar geochemical composition; and group one samples are mainly concentrated in this region (Fig. 4a). Because of the wind ablation on the Ordos Plateau, 'hard ridges' stretched from the Ordos Plateau into the depression, where Cretaceous and Jurassic sandstone are subjected to weathering and produce sand sources for these dunefields. Local sand sources and the recycling of Cretaceous eolian material may control the chemical compositions of these dunefields (Dong and Li, 1986). Recent zircon U–Pb dating and rare earth element results support this explanation (Rao et al., 2011; Stevens et al., 2010).

Active dunefields represented by group 2, located in the southern Mu Us Desert depression, are characterized by higher Ni, Go, and Ge contents (Fig. 4b and c). We suggest that the eolian sediments, derived from a long-distance transport source, and reworked sands underlying the fluvial formation, such as the Chengchuan Formation, also provided the provenance for these dunefields. Active dunefields (Fig. 4b) in the southwestern sector of the Mu Us Desert have been suggested to have derived from sources in the Yellow River and its tributary valleys (Stevens et al., 2010). However, we are not able to confirm the Yellow River valley origin at this stage because our limited data could not capture specific changes of chemical properties. The sands of group three are mainly distributed in the boundary between those of group one and group two (Fig. 4d). This indicates a mixing effect between these two groups.

Then discussion the next important factor is the sorting process. Previous studies of the loess-paleosol sequence in the Chinese Loess Plateau show strong partitioning of certain elements and minerals into different grain-size fractions, which suggests that wind sorting may have significantly contributed to the element and mineral compositions (Yang et al., 2006). By comparing the bulk chemical composition with different grain-size fractions, we evaluated the wind sorting effect on the elemental and mineral compositions. We correlated the measured elemental concentrations with the sand, silt, and clay fractions as well as the sand mean particle size and standard deviation. For 41 samples ($n = 41$), the correlation coefficient was significant at the 0.01 confidence level, with an absolute p value of 0.38. We found that the concentration of Si, Fe, Ca, Mg, Ti, Cr, V, Cu, Zr, and Nb were more closely linked to the absolute value of the correlation coefficient. The elements Al, K, Na, Co, Ni, Ga, Ge, Rb, Sr, and Ba showed weak correlations between the mean grain size and sorting factor, implying an insignificant linkage.

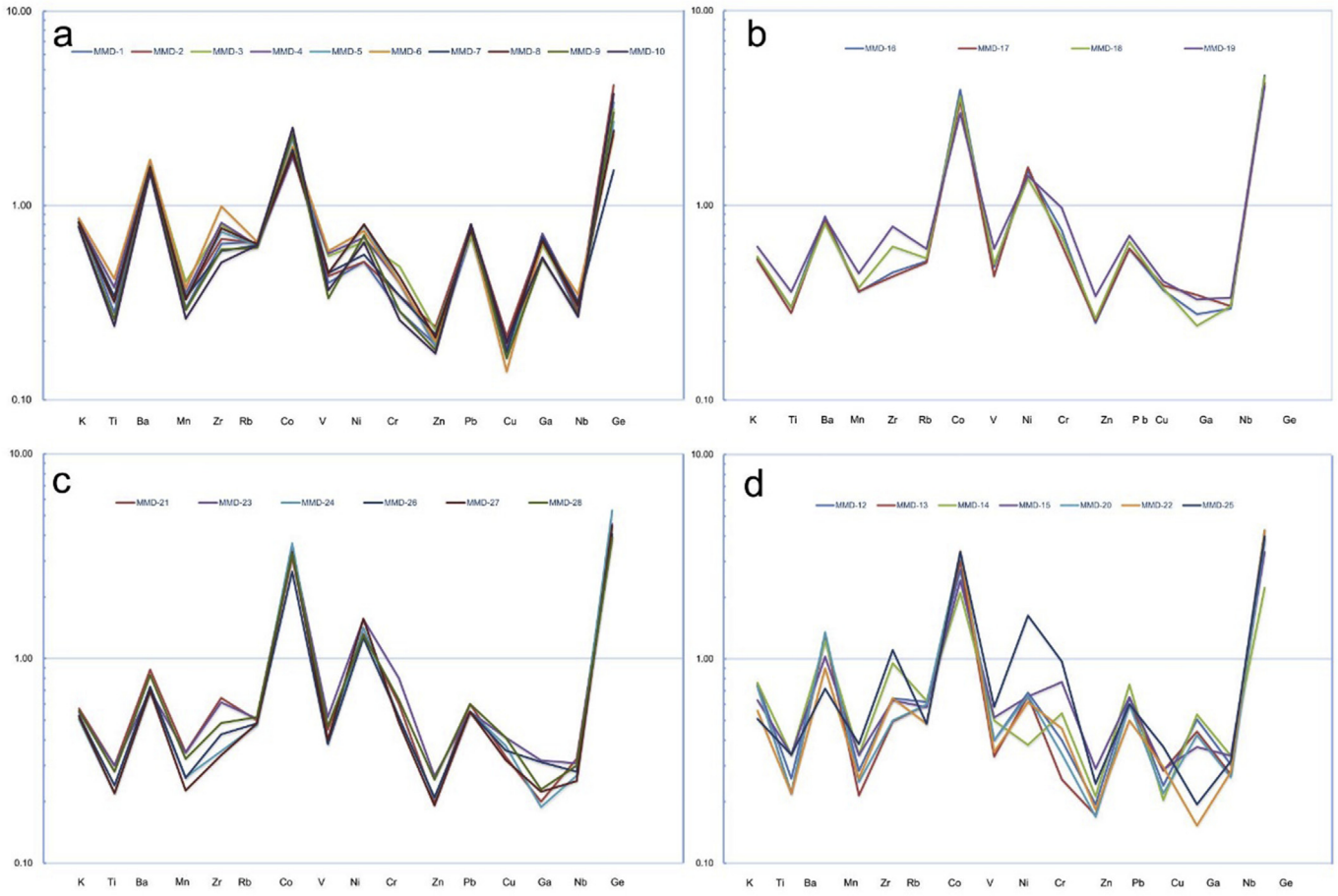


**Fig. 4.** UCC-normalized elements values of dune sand samples from the Mu Us Desert.

**Table 3**
Correlation between the elements and grain size of the sand, silt, and clay fractions as well as the descriptive parameters of the grain-size distribution (Mz, σ).

| Element | Clay | Silt | Very fine sand | Fine sand | Medium sand | Coarse sand | Very coarse sand | Mz (Φ) | σ (Φ) |
|---|---|---|---|---|---|---|---|---|---|
| $SiO_2$ | −0.72 | −0.66 | −0.71 | 0.48 | 0.43 | **−0.14** | −0.39 | −0.60 | −0.66 |
| $Al_2O_3$ | 0.49 | 0.38 | 0.42 | −0.55 | −0.04 | **0.31** | **0.28** | **0.23** | 0.42 |
| $Fe_2O_3$ | 0.60 | 0.72 | 0.75 | −0.06 | −0.79 | **−0.32** | 0.37 | 0.85 | 0.62 |
| CaO | 0.59 | 0.75 | 0.76 | −0.52 | −0.45 | **0.06** | **0.31** | 0.69 | 0.71 |
| $Na_2O$ | **0.05** | **−0.06** | **−0.03** | −0.46 | 0.44 | **0.36** | **0.05** | **−0.26** | **0.03** |
| MgO | **0.31** | 0.59 | 0.58 | **0.03** | −0.69 | **−0.33** | **0.16** | 0.73 | 0.50 |
| $K_2O$ | **0.25** | **0.10** | **0.11** | −0.62 | 0.35 | 0.51 | 0.15 | **−0.15** | **0.23** |
| $TiO_2$ | 0.64 | 0.66 | 0.71 | −0.26 | −0.55 | **−0.18** | 0.43 | 0.69 | 0.61 |
| Ba | **0.24** | **0.06** | **0.05** | −0.63 | 0.42 | 0.53 | 0.15 | **−0.21** | **0.21** |
| Sr | **0.21** | **0.07** | **0.09** | −0.60 | 0.39 | 0.42 | 0.15 | **−0.17** | **0.19** |
| Zr | 0.64 | 0.64 | 0.76 | −0.38 | −0.49 | **−0.04** | 0.50 | 0.62 | 0.62 |
| Rb | 0.53 | 0.43 | 0.46 | −0.60 | **−0.06** | **0.35** | 0.26 | **0.27** | 0.50 |
| Co | **−0.22** | **−0.19** | **−0.19** | 0.45 | **−0.14** | **−0.33** | −0.03 | **−0.04** | **−0.21** |
| V | 0.62 | 0.70 | 0.82 | **−0.19** | −0.68 | **−0.28** | 0.37 | 0.79 | 0.58 |
| Ni | **−0.10** | **−0.12** | **−0.03** | 0.50 | **−0.28** | −0.49 | −0.03 | **0.14** | **−0.20** |
| Cr | 0.50 | 0.67 | 0.76 | **0.06** | −0.85 | −0.42 | 0.30 | 0.86 | 0.53 |
| Cu | **0.19** | 0.39 | 0.42 | **0.32** | −0.72 | −0.44 | 0.00 | 0.63 | **0.23** |
| Ga | 0.41 | **0.29** | **0.29** | −0.64 | **0.17** | 0.41 | 0.22 | **0.06** | 0.38 |
| Nb | 0.61 | 0.72 | 0.81 | **−0.17** | −0.72 | **−0.25** | 0.36 | 0.82 | 0.60 |
| Ge | **−0.26** | **−0.27** | **−0.31** | 0.37 | **0.01** | **−0.13** | −0.08 | **−0.18** | **−0.17** |

The bold numbers indicate an insignificant correlation coefficient.

### 5.2. Geochemical proxies for the environment

Because different provenance sediment have effects on the element compositions of different grain-size fractions, we chose samples from different dunefields where share some provenance and used elements ratios, which are less sensitive to grain-size fractions, to examine whether environment controls the current elemental compositions of the Mu Us Desert. We choose stabilized dunefields are located in the downwind direction from active dunefields, both stabilized and active dunefields supposed have the same provenance. It is well established that the 'Sr-type' and 'Na-type' elemental ratios are servel proxies, which are more or less independent from the provenance factor and have less influence by sorting (Chen et al., 1999).

The Rb/Sr and Ba/Sr ratios belong to the 'Sr-type' indexes that are widely used to evaluate the chemical weathering intensity. The Rb/Sr ratio also relies on the facts that Sr will replace Ca and shows a behavior similar to that of Ca in a weathering section. Due to strong adsorption by clay minerals in the course of weathering, Rb and Ba are relatively immobile under moderate weathering conditions, whereas Sr is soluble and easily mobilized (McLennan et al., 1993; Nesbitt and Markovics, 1980). Thus, with increasing weathering intensity, the Ba/Sr and Rb/Sr ratios increase.

The most prominent 'Na-type' indexes representing feldspar weathering are CIW (Harnois, 1988), CIA (Nesbitt and Young, 1982), CPA(Buggle et al., 2011), WPI(Parker, 1970) and Na/K (Table 4). These ratios rely on the fact that Na can be easily released from minerals (such as plagioclase) and will be mobilized. As a result, Al is enriched in situ by forming secondary clay minerals and/or Al-oxides, such as illite. Thus, 'Na-type' indexes are used to measure the magnitude of feldspar weathering. All of these indexes are calculated in molar contents, and CaO* refers to CaO in silicate. According to the different test conditions and research objectives, the calculation and correction of CaO* can differ. Here, we used the following equation: $CaO^* = 0.35 \times 2(Na_2O\ wt\%)/62$, which was proposed by Honda and Shimizu (1998), to calculate CIA for Taklamakan Desert sediments.

**Table 4**
Weathering indexes (molecular proportions).

| |
|---|
| WIP[a] = 100*[(2*$Na_2O$/0.35) + (MgO/0.9)+(2*$K_2O$/0.25) + (CaO/0.7)] |
| CIA[b] = [$Al_2O_3$/($Al_2O_3$ + $Na_2O$ + CaO*+$K_2O$)]*100 |
| CIW[c] = [$Al_2O_3$/($Al_2O_3$ + $Na_2O$ + CaO*)] *100 |
| CPA[d] = [$Al_2O_3$/($Al_2O_3$ + $Na_2O$)] *100 |

[a] Weathering Index of Parker (1970).
[b] Chemical index of alteration (Nesbitt and Young, 1982).
[c] Chemical index of weathering (Harnois, 1988).
[d] Chemical proxy of alteration (Buggle et al., 2011).

The selected single 'Sr-type' and 'Na-type' element ratio indexes (Na/K,Rb/Sr,Ba/Sr) for eolian sand are plotted as empirical weathering progress diagrams in Fig. 5. The 'Sr-type' and 'Na-type' indexes of the surface sediments in the Mu Us Desert show a relatively higher weathering intensity at stabilized and semi-stabilized dunefields than at active dunefields. However, due to the different provenance, some indexes obtained from the active dunefield samples show somewhat stronger weathering intensities than those of the stabilized and semi-stabilized dunefield samples (Fig. 5). In this case, some of the elemental ratios were inherited from their parent rocks, which simply reflect variations of their bulk chemistry and the mineralogy of the source areas before transportation, superposed on the weathering indexes, though the provenance been supposed same. In addition, several mineral will be enrichment by eolian sorting can change this ratio value.

A complicated weathering index is developed on a heterogeneous provenance indicates a mixture of weathering intensity, parent rock geochemistry and sorting effect.We applied and plotted almost all of the weathering indexes, such as CIA, WIP, CIW, and CPA, which are defined in Table 3, with latitudinal changes to discuss the spatial changes and to check the index suitability for dune sand weathering (Fig. 6). Fig. 6 shows that with the increase of latitude, the WIP values increase, while the CIA, CIW, and CPA values decrease, suggesting that the weathering intensity became weaker, although it fluctuated. The four indexes indicate that stabilized/semi-stabilized dunefields and active dunefields have different weathering intensity signatures and show the tendency of northwesterward desertification. The Asian Summer monsoon climate delivers lesser tendency heat and rainfall from southeastern to northwestern China, leading the weathering intensity in the Mu Us Desert to have a fixed spatial pattern, accordingly. By analyzing the relationship between the weathering intensity and site latitude, we observed that WIP has the highest correlation coefficient ($R^2 = 0.67$). The WIP index suggests that the modern climate affected the Mu Us Desert significantly. We conclude that the WIP index shows the clearest weathering signal at here. To

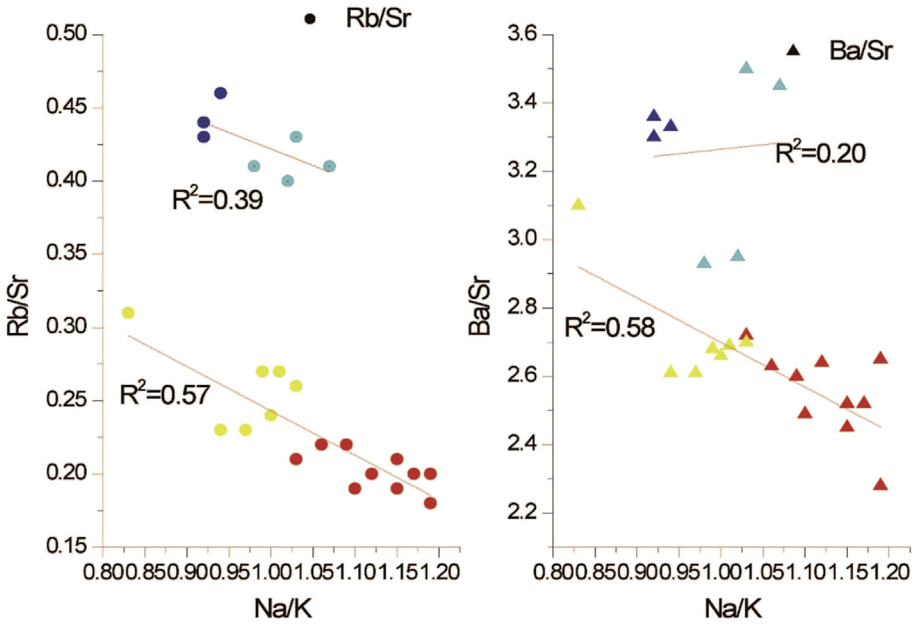


**Fig. 5.** . 'Sr-type' and 'Na-type' indexes for the selected eolian sand sample empirical weathering progress diagrams. Red samples are MMD1 to MMD10, yellow samples are MFD1 to MFD7, light blue samples are MMD16-MMD19, and dark blue samples are MFD8 to MFD10. (For interpretation of the references to colour in this figure legend, the reader is referred to the web version of this article.)

characterize the weathering profiles of felsic, heterogeneous, metasedimentary bedrocks in North Carolina, Price and Velbel (2003) compared several weathering indexes and indicated that the WIP index also is the most appropriate index of alteration for application to felsic, heterogeneous, weathered regoliths. Overall, one should be cautious in interpreting the weathering intensity at a desert eolian deposition site just using single 'Sr-type' and 'Na-type' elemental ratios when the provenance geochemistry background is unknown/unclear.

### 5.3. Implications for reconstructing the paleoenvironment

One excellent dune sand–paleosol succession was identified from an outcrop in the Mu Us Desert, and been called shenmu section here, which provided an ideal stratigraphic framework for reconstructing the paleoclimate and servel. We compared the Mz(ϕ)-major elements, Mz(ϕ)-CIA and Mz(ϕ)-OM(‰) (organic matter), between paleo-dune sand/paleosol samples and surface-active/stabilized and semi-stabilized dune sand (Fig. 7). The paleo-dune sand/paleosol samples and surface active/stabilized and semi-stabilized dune sand are clearly identifiable using a scatter diagram. Paleosol and surface-stabilized and semi-stabilized dune sands have similar grain size characteristics and organic matter contents. More than half of the paleosol samples show chemical ratios and grain-size fractions in the range of surface-stabilized and semi-stabilized dune sand (Fig. 7). Regardless of an ancient or modern origin, dune sand samples are characterized by higher Si and Na and lower Al and Fe contents. However, the Si, Na, and Fe contents in the paleosol and surface-stabilized and semi-stabilized dune sands are the reverse. We propose that the chemical ratios of stabilized and semi-stabilized dune sand are analogous to buried sandy paleosols and that the chemical ratios of modern active dune sand are analogous to that of paleo-dune sand. The chemically stable major element contents in paleosols should be higher than those in dune sand. Except for Si, the contents of chemically stable major elements, such as Al, Fe, and Ti, exhibit high value peaks in paleosols (Fig. 8). However, Ca and Mg, which are chemically mobile major elements, also show high content peaks in paleosols, whereas the Na and K contents are low. This phenomenon is caused by relatively weak pedogenic processes because Ca and Mg are relatively enriched after leaching and translocation of Na and K. In addition, paleo-dune sand shows a high abundance of the chemically stable major element Si, while Al, Fe, Ti, Ca, and Mg a reduced in paleo-dune sand. This finding indicates that the Si content in paleo-dune sand diluted other elements during dune sand formation.

The alternation of dune sands and paleosols in the shenmu section is clearly expressed in the major elements ratios (Fig. 8), with paleosol exhibiting lower Si, Mg, Na, and WIP values and higher Al, Fe, Ca, K, Ti, CIW, CPA, and CIA values than the adjacent sands units. The major elements values display a jagged change with increased or decreased contents (Fig. 8). On the other hand, the CIW, CPA, CIA, and WIP ratios show relatively smooth fluctuations, in phase with the paleo-dune and paleosol stratigraphic changes. The variation of the major elements may be influenced by pedogenesis and biochemical weathering in this section. This may be related to the fact that CIW, CPA, CIA, and WIP incorporate Ca, Na, Al, and K, rather than a single element, into the calculations (Nesbitt and Young, 1982). The comparison of the weathering proxies with the major elements of the shenmu section further suggests that CIW, CPA, CIA, and WIP are robust proxies for the chemical weathering intensity. Although the WIP index is not very different from those of the other three indexes, it appears that the provenance is constant during this period.

Here, the CIA, CIW, CPA, and WIP values will be used as indicators of the intensity of the variation of ASM and AWM. The present climate in the Mu Us Desert is mainly controlled by the ASM and AWM systems. During local summer and fall, approximately from June to October, the formation of a high pressure cell over the Pacific Ocean and a low pressure cell over the Asian continent produces a pressure gradient between the ocean and land that forces a steady flow of moist maritime air from the southeast towards the interior of the continent, known as the ASM (Wang, 2006). This flow frequently reaches the Chinese Loess

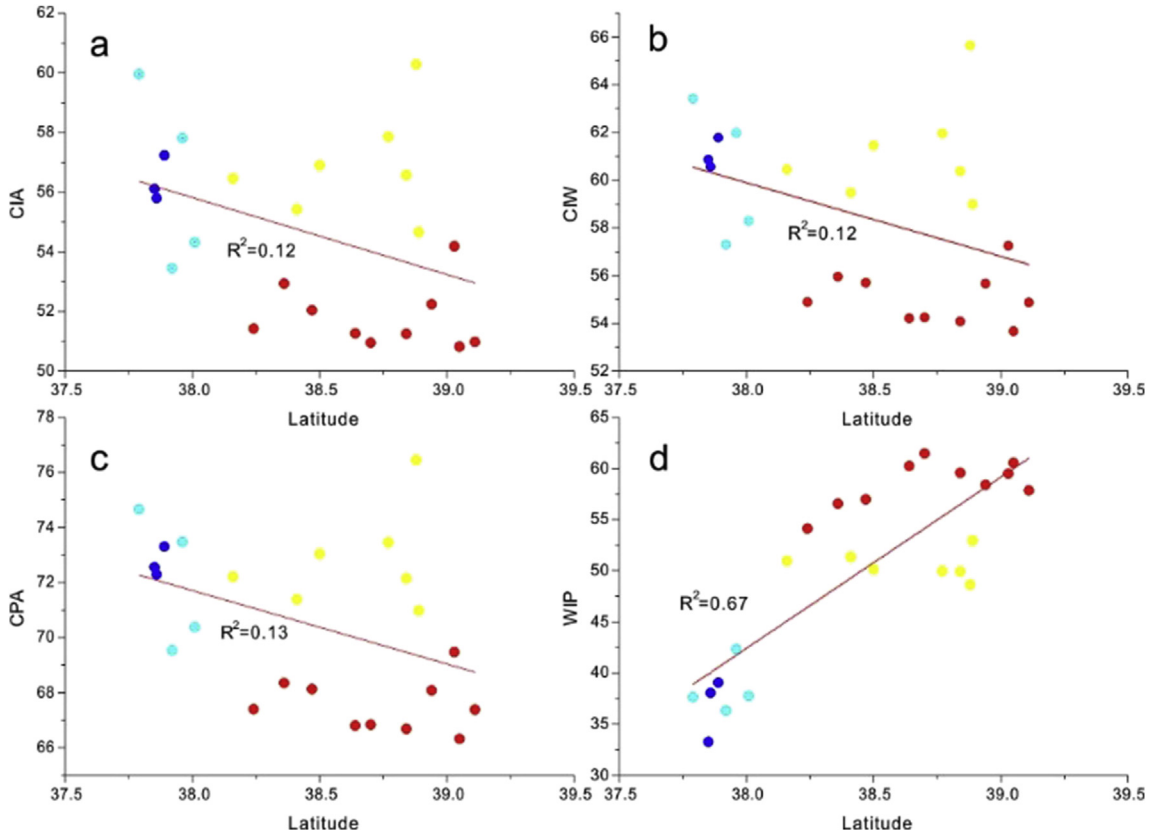


**Fig. 6.** Weathering indexes CIA (a), CIW (b), CPA (c), and WIP (d) for the selected eolian sand samples with latitudinal change diagrams. Red samples are MMD1 to MMD10, yellow samples are MFD1 to MFD7, light blue samples are MMD16-MMD19, and dark blue samples are MFD8 to MFD10. (For interpretation of the references to colour in this figure legend, the reader is referred to the web version of this article.)

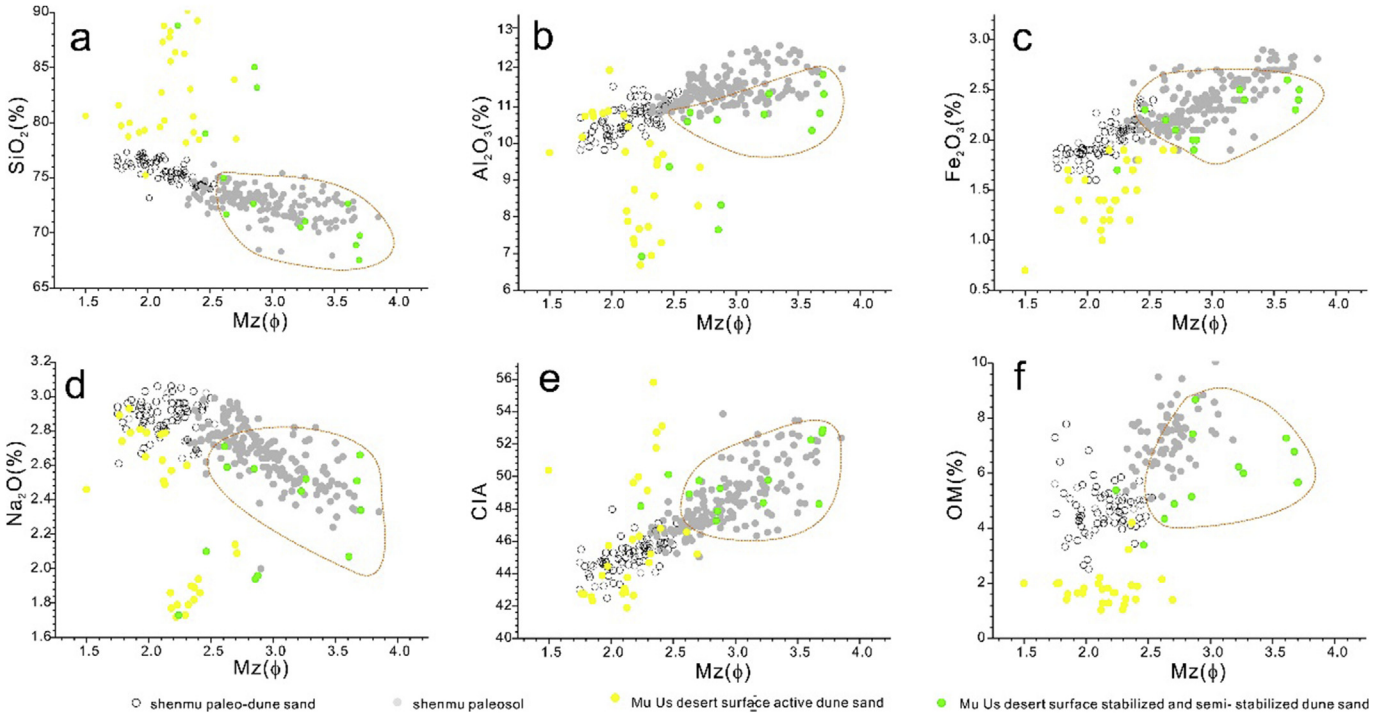


**Fig. 7.** Comparison of the Mz(ϕ) and major elements between paleo-dune sand/paleosol and surface active/stabilized and semi-stabilized dune sand. (a is Mz(ϕ) vs. Si, b is Mz(ϕ) vs Al, c is Mz(ϕ) vs Fe, d is Mz(ϕ) vs Na, e is Mz(ϕ) vs CIA and f is Mz(ϕ) vs organic matter (OM)).

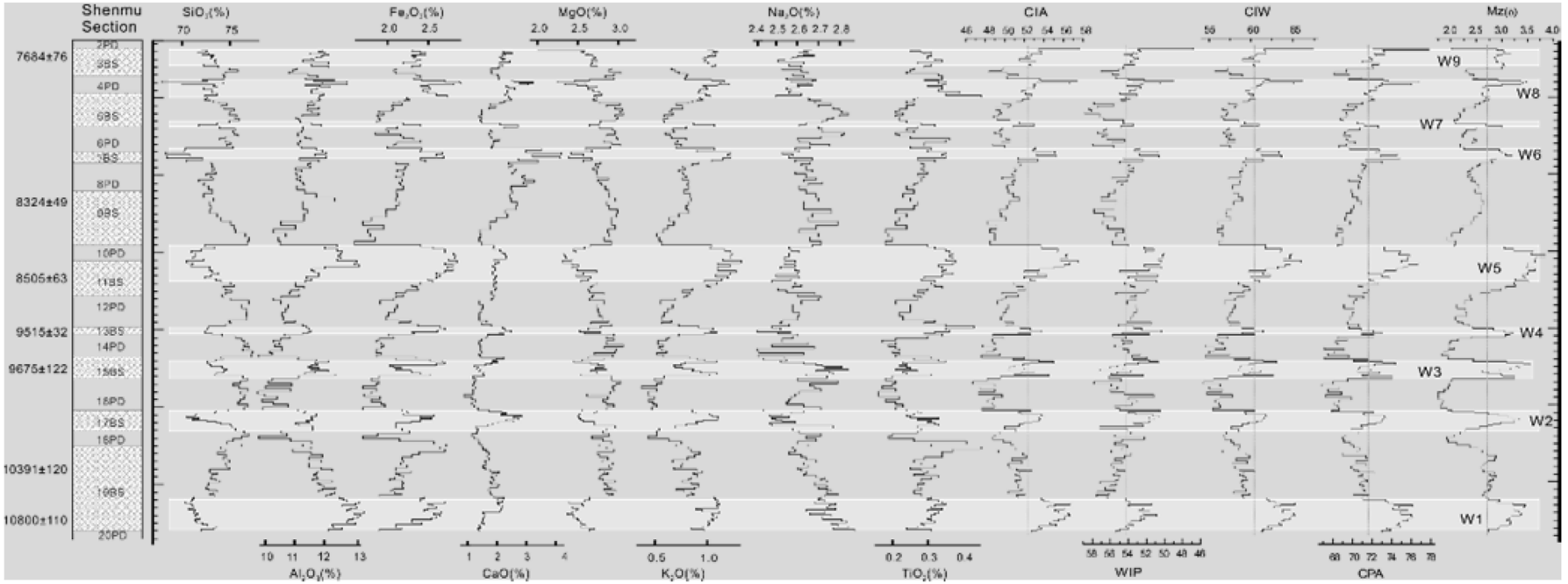


**Fig. 8.** Major elements and element ratio curves of the shenmu section and the paleoenvironment change during the early Holocene ('W' represent the wet period).

Plateau and desert–loess transition belt region, where it increases precipitation and thermal energy (An et al., 1991; Dong et al., 1998; Sun and Ding, 1998; Zhou et al., 2002). Hence, intensified ASM conditions directly the vegetation cover and stabilize the sandy land surface, favoring grassland soil formation, known as modern sandy black loam. A more stabilized land surface due to the relatively healthy vegetation coverage increases the dust trapping efficiencies, facilitating the capture of finer windborne dusts. In this situation, high values of CIA, CIW, and CPA and low values of WIP in this dune–paleosol succession suggest a strong ASM northwestward migration into the Mu Us Desert region, stabilizing the dunefields through surface soil formation (marked W1–W9 in Fig. 8).

During extended winter and spring from November to May, a high pressure cell, developed over north-central Asia, and a low pressure cell, formed over the west Pacific Ocean, produce a pressure gradient, resulting in a cold and dry airflow from the Siberia–Mongolia high-pressure cell region southeastward, known as the AWM. The winter climate in the Mu Us Desert is cold, dry, and windy. Most plants cannot survive, and the sandy land surface becomes uncovered. The unstabilized land surface provides eolian sources, and northwesterly wind transports loose particles southeastward. The desert–loess transition belt is thus dominated by winds from the north and/or northwest, which generate dust storms and cause downwind deposition of dunefields (Dong et al., 1998; Sun and Ding, 1998; Zhou et al., 2002). The coarse sand grains deposit first during transportation, close to their source, followed by progressively smaller grains, ranging from finer sand to silt and clay particles, moving farther away from the source areas into the Chinese Loess Plateau. The lower values of CIA, CIW, and CPA and higher values of WIP suggest a strong AWM, intensifying the eolian sand activity and destabilizing the land surface. The preliminary geochemical study on this excellent dune–paleosol succession reveals that the strong ASM and AWM periods could have recurred 8–9 times during the early Holocene in the Mu Us Desert.

## 6. Conclusions

The Mu Us Desert is one of the key regions for studying the history of the eolian sand activity and the evolution of the desert in northern China. We present a new dataset from 28 active and 13 stabilized–semi stabilized dunefields in the Mu Us Desert to report dune sand chemical properties at the macroscopic scale. We also reveal the relationship between various chemical ratio indexes and modern climate conditions for different types of the Mu Us sandy landscapes. We conclude:

(1) The geochemical composition of the surface sand samples from the Mu Us Desert is dominated by Si and Al; the Zr, Ba and Sr contents are higher than those of any other trace elements.
(2) The major element contents from the active and stabilized and semi-stabilized dunefields differ in certain ways. The Si content of the active dunefields is 7.5% higher than that of the stabilized and semi-stabilized dunefields, and the contents of Al, Fe, Ca, Mg, and Ti are lower in active dunefields than in stabilized and semi-stabilized dunefields.
(3) Compared with the average chemical composition of major elements, Si is enriched and other elements are depleted in the UCC; compared with the average chemical composition of trace elements, Ba, Co, and Ge are relatively enriched and other trace elements are relatively depleted.
(4) The geochemical proxies obtained from the eolian deposit–paleosol records, such as the CIA, CIW, CPA, and WIP chemical weathering indexes, can provide useful information for the reconstruction of the servel. However, one should be cautious in interpreting the weathering intensity at a depositional site using element ratios when their provenance geochemistry background is unknown
(5) The preliminary geochemical study implies that modern sandy soil is analogous to buried paleosol, whereas paleodune sand is similar to modern active dune sand. The weathering indexes of an excellent dune–paleosol succession reveal that strong ASM and AWM periods could have recurred 8–9 times during the Holocene epoch in the Mu Us Desert.

## Acknowledgements

This study was supported by National Basic Research Program of China, Grant Number:2013CB955903; National Natural Science Foundation of China, Grant Number:41290250; the External Cooperation Program of BIC, Chinese Academy of Sciences, Grant Number:132B61KYSB20130003 and Scientific Research Foundation of Graduate School of South China Normal University (2013kyjj040).

## References

An, Z., Kukla, G.J., Porter, S.C., Xiao, J., 1991. Magnetic susceptibility evidence of monsoon variation on the Loess Plateau of central China during the last 130,000 years. Quat. Res. 36, 29–36.
Buggle, B., Glaser, B., Hambach, U., Gerasimenko, N., Marković, S., 2011. An evaluation of geochemical weathering indices in loess–paleosol studies. Quat. Int. 240, 12–21.
Chen, J., An, Z., Head, J., 1999. Variation of Rb/Sr ratios in the loess-paleosol sequences of Central China during the last 130,000 years and their implications for monsoon paleoclimatology. Quat. Res. 51, 215–219.
Chen, J., An, Z., Liu, L., 2001. Variations in chemical compositions of the eolian dust in Chinese Loess Plateau over the past 2.5 Ma and chemical weathering in the Asian inland. Sci. China (Ser. D) 44, 403–413.
Ding, Z.L., Sun, J.M., Rutter, N.W., Rokosh, D., Liu, T.S., 1999. Changes in sand content of loess deposits along a north-south transect of the Chinese Loess Plateau and the implications for desert variations. Quat. Res. 52, 56–62.
Dong, G.R., 2002. Climate and Environment Changes in Deserts of China—Selected Papers of Dong Guangrong's Research Group (in Chinese). China Ocean, Beijing.
Dong, G., Li, B., 1986. The Relationship of the Malan Loess along the Salawusu River with the Salawusu Formation in Inner Mongolia and its Environmental evolution, Geological and Environmental Evolutions of Qaidam Basin, Qinghai Province in the Late Cenozoic. Science Press of China, Beijing, pp. 86–116.
Dong, G.R., Wang, G.Y., Li, X.Z., Chen, H.Z., Jin, J., 1998. Palaeomonsoon vicissitudes in eastern desert region of China since last interglacial period. Sci. China Ser. D. 41, 215–224.
Dong, G.R., Li, B.S., Gao, S.Y., Wu, Z., Shao, Y.J., 1983. The Quaternary ancient eolian sands in the Ordos Plateau. Acta Geographica Sinica 4, 341–347.
Duller, G.A.T., 2016. Challenges involved in obtaining luminescence ages for long records of aridity: examples from the Arabian Peninsula. Quat. Int. 410, 69–74.
Fitzsimmons, K.E., Cohen, T.J., Hesse, P.P., Jansen, J., Nanson, G.C., May, J.H., Barrows, T.T., Haberlah, D., Hilgers, A., Kelly, T., Larsen, J., Lomax, J., Treble, P., 2013. Late quaternary palaeoenvironmental change in the Australian drylands. Quat. Sci. Rev. 74, 78–96.
Folk, P.L., Ward, W.D., 1957. Brazos Reviver bar: a study in the significance of grain size parameters. J. Sediment. Petrol. 27, 3–26.
Halfen, A.F., Lancaster, N., Wolfe, S., 2016. Interpretations and common challenges of aeolian records from North American dune fields. Quat. Int. 410, 75–95.
Harnois, L., 1988. The CIW index: a new chemical index of weathering. Sediment. Geol. 55, 319–322.
He, Z., Zhou, J., Lai, Z., Yang, L., Liang, J., Long, H., Ou, X., 2010. Quartz OSL dating of sand dunes of late pleistocene in the Mu Us desert in northern China. Quat. Geochronol. 5, 102–106.
Honda, M., Shimizu, H., 1998. Geochemical, mineralogical and sedimentological studies on the Taklimakan Desert sands. Sedimentology 45, 1125–1143.
Jia, F., Lu, R., Gao, S., Li, J., Liu, X., 2015. Holocene aeolian activities in the southeastern Mu Us desert, China. Aeolian Res. 19, 267–274.
Lancaster, N., 2008. Desert dune dynamics and development: insights from lumines cence dating. BOREAS 37, 559–573.
Lancaster, N., Yang, X., Thomas, D., 2013. Spatial and temporal complexity in quaternary desert datasets: implications for interpreting past dryland dynamics and understanding potential future changes. Quat. Sci. Rev. 78, 301–302.
Li, B.S., Gao, S., Dong, G., Jin, H., 2005. The environmental evolution of Ordos desert, China since 1.1 Ma B. P. As indicated by yulin stratigraphical section and its grain-size analysis results. Chin. Geogr. Sci. 15, 34–41.

Li, B.S., Zhang, D.D., Jin, H.L., Wu, Z., Yan, M.C., Wu, S., Zhu, Y.Z., Sun, D.H., 2000. Paleo-monsoon activities of Mu Us Desert, China since 150 ka BP - a study of the stratigraphic sequences of the milanggouwan section, Salawusu river area. Palaeogeogr. Palaeocl. 162, 1–16.
Li, G., Ji, J., Zhao, L., Mao, C., Chen, J., 2008. Response of silicate weathering to monsoon changes on the Chinese Loess Plateau. Catena 72, 405–412.
Li, H., Yang, X., 2016. Spatial and temporal patterns of aeolian activities in the desert belt of northern China revealed by dune chronologies. Quat. Int. 410, 58–68.
Li, S.H., Sun, J.M., Li, B., 2012. Holocene environmental changes in central Inner Mongolia revealed by luminescence dating of sediments from the Sala Us river valley. Holocene 22, 397–404.
Liu, B., Jin, H., Sun, L., Sun, Z., Niu, Q., Xie, S., Li, G., 2014. Holocene moisture change revealed by the Rb/Sr ratio of aeolian deposits in the southeastern Mu Us Desert, China. Aeolian Res. 13, 109–119.
Liu, D.S., Sun, J.M., 2002. Expansion and contraction of Chinese deserts during the quaternary. Sci. China Ser. D. 45, 91–101.
Liu, K., Lai, Z.P., 2012. Chronology of Holocene sediments from the archaeological Salawusu site in the Mu Us desert in China and its palaeoenvironmental implications. J. Asian Earth Sci. 45, 247–255.
Lu, H., Zhou, Y., Liu, W., Mason, J., 2012. Organic stable carbon isotopic composition reveals late quaternary vegetation changes in the dune fields of northern China. Quat. Res. 77, 433–444.
Lu, H.Y., Miao, X.D., Zhou, Y.L., Mason, J., Swinehart, J., Zhang, J.F., Zhou, L.P., Yi, S.W., 2005. Late quaternary aeolian activity in the Mu Us and Otindag dune fields (north China) and lagged response to insolation forcing. Geophys Res. Lett. 32.
McLennan, S., Hemming, S., McDaniel, D., Hanson, G., 1993. Geochemical approaches to sedimentation, provenance, and tectonics. Geol. Soc. Am. Spec. Pap. 284, 21–40.
Nesbitt, H., Young, G., 1982. Early Proterozoic climates and plate motions inferred from major element chemistry of lutites. Nature 299, 715–717.
Nesbitt, H.W., Markovics, G., 1980. Chemical processes affecting alkalis and alkaline earths during continental weathering. Geochim. et Cosmochim. Acta 44, 1659–1666.
Parker, A., 1970. An index of weathering for silicate rocks. Geol. Mag. 107, 501–504.
Price, J.R., Velbel, M.A., 2003. Chemical weathering indices applied to weathering profiles developed on heterogeneous felsic metamorphic parent rocks. Chem. Geol. 202, 397–416.
Rao, W., Chen, J., Tan, H., Jiang, S., Su, J., 2011. Sr–Nd isotopic and REE geochemical constraints on the provenance of fine-grained sands in the Ordos deserts, north-central China. Geomorphology 132, 123–138.
Stevens, T., Palk, C., Carter, A., Lu, H., Clift, P.D., 2010. Assessing the provenance of loess and desert sediments in northern China using U-Pb dating and morphology of detrital zircons. Geol. Soc. Am. Bull. 122, 1331–1344.
Sun, J.M., Ding, Z.L., 1998. Deposits and soils of the past 130,000 years at the desert-loess transition in northern China. Quat. Res. 50, 148–156.
Sun, J.M., Ding, Z.L., Liu, T.S., Rokosh, D., Rutter, N., 1999. 580,000-year environmental reconstruction from aeolian deposits at the Mu Us Desert margin, China. Quat. Sci. Rev. 18, 1351–1364.
Taylor, S.R., McLennan, S.M., 1985. The continental crust: its composition and evolution. The Journal of Geology.
Telfer, M.W., Hesse, P.P., 2013. Palaeoenvironmental reconstructions from linear dunefields: recent progress, current challenges and future directions. Quat. Sci. Rev. 78, 1–21.
Thomas, D.S.G., Burrough, S.L., 2012. Interpreting geoproxies of late quaternary climate change in African drylands: implications for understanding environmental change and early human behaviour. Quat. Int. 253, 5–17.
Thomas, D.S.G., Burrough, S.L., 2013. Luminescence-based dune chronologies in southern Africa: analysis and interpretation of dune database records across the subcontinent. Quat. Int. 1–16.
Wang, B., 2006. The Asian Monsoon. Springer Science & Business Media.
Wang, H., Liu, L., Feng, Z., 2008. Spatiotemporal variations of Zr/Rb ratio in three last interglacial paleosol profiles across the Chinese Loess Plateau and its implications for climatic interpretation. Sci. Bull. 53, 1413–1422.
Wen, X., Li, B., Zheng, Y., Yang, Q., Niu, D., Shu, P., 2016. Early Holocene multi-centennial moisture change reconstructed from lithology, grain-size and chemical composition data in the eastern Mu Us desert and potential driving forces. Palaeogeogr. Palaeoclimatol. Palaeoecol. 459, 440–452.
Wu, Z., 2009. Sandy deserts and its Control in China. Science Press, Beijing China.
Xu, Z., Lu, H., Yi, S., Vandenberghe, J., Mason, J.A., Zhou, Y., Wang, X., 2015a. Climate-driven changes to dune activity during the last glacial maximum and deglaciation in the Mu Us dune field, north-central China. Earth Planet. Sci. Lett. 427, 149–159.
Xu, Z., Mason, J.A., Lu, H., 2015b. Vegetated dune morphodynamics during recent stabilization of the Mu Us dune field, north-central China. Geomorphology 228, 486–503.
Yang, S., Ding, F., Ding, Z., 2006. Pleistocene chemical weathering history of Asian arid and semi-arid regions recorded in loess deposits of China and Tajikistan. Geochim. et Cosmochim. Acta 70, 1695–1709.
Zhou, W.J., Dodson, J., Head, M.J., Li, B.S., Hou, Y.J., Lu, X.F., Donahue, D.J., Jull, A.J.T., 2002. Environmental variability within the Chinese desert-loess transition zone over the last 20 000 years. Holocene 12, 107–112.
Zhu, Z., Wu, Z., Liu, S., 1980. An Outline on Chinese Deserts. Science Press, Beijing.